# Relativistic Coulomb excitation of neutron-rich $^{54,56,58}$Cr: On the pathway of magicity from N=40 to N=32

A. Bürger [a], T.R. Saito [b], H. Grawe [b], H. Hübel [a,*], P. Reiter [c], J. Gerl [b], M. Górska [b], H.J. Wollersheim [b] A. Al-Khatib [a], A. Banu [b], T. Beck [b], F. Becker [b], P. Bednarczyk [b,d], G. Benzoni [e], A. Bracco [e] , S. Brambilla [e], P. Bringel [a], F. Camera [e], E. Clément [f], P. Doornenbal [c], H. Geissel [b], A. Görgen [f], J. Grębosz [b,d], G. Hammond [g], M. Hellström [b], M. Honma [h], M. Kavatsyuk [b,i], O. Kavatsyuk [b,i], M. Kmiecik [d], I. Kojouharov [b], W. Korten [f], N. Kurz [b], R. Lozeva [b,j], A. Maj [d], S. Mandal [b], B. Million [e], S. Muralithar [k], A. Neußer [a], F. Nowacki [ℓ], T. Otsuka [m,n], Zs. Podolyák [o], N. Saito [b], A.K. Singh [a,p], H. Weick [b], C. Wheldon [q], O. Wieland [e], M. Winkler [b] and the RISING collaboration

[a] *Helmholtz-Institut für Strahlen- und Kernphysik, Universität Bonn, Germany*

[b] *Gesellschaft für Schwerionenforschung (GSI), Darmstadt, Germany*

[c] *Institut für Kernphysik, Universität zu Köln, Germany*

[d] *The Henryk Niewodniczański Institute of Nuclear Physics, PAN, Kraków, Poland*

[e] *Dipartimento di Fisica, Università di Milano, and INFN sezione di Milano, Italy*

[f] *DAPNIA/SPhN, CEA Saclay, Gif-sur-Yvette, France*

[g] *Department of Physics, Keele University, Keele, UK*

[h] *University of Aizu, Fukushima 965-8580, Japan*

[i] *Taras Shevchenko Kiev National University, Ukraine*

[j] *Faculty of Physics, University of Sofia, Bulgaria*

[k] *Nuclear Science Centre, New Delhi, India*

[ℓ] *IReS, Université Louis Pasteur, Strasbourg, France*

[m] *Department of Physics, University of Tokyo, Japan*

[n] *RIKEN, Hirosawa, Japan*

[o] *Department of Physics, University of Surrey, UK*

[p] *Department of Physics & Meteorology, Indian Institute of Technology Kharagpur,*

*Preprint submitted to Elsevier Science* *15 June 2005*

*Kharagpur - 721302, India*
[q]*SF7, Hahn-Meitner-Institut, Berlin, Germany*

**Abstract**

The first excited $2^+$ states in $^{54,56,58}$Cr were populated by Coulomb excitation at relativistic energies and $\gamma$ rays were measured using the RISING setup at GSI. For $^{56}$Cr and $^{58}$Cr the $B(E2, 2_1^+ \rightarrow 0^+)$ values relative to the previously known $B(E2)$ value for $^{54}$Cr are determined as 8.7(3.0) and 14.8(4.2) W.u., respectively. The results are consistent with a subshell closure at neutron number $N = 32$ which was already indicated by the higher energy of the $2_1^+$ state in $^{56}$Cr. Recent large-scale shell model calculations using effective interactions reproduce the trend in the excitation energies, but fail to account for the minimum in the $B(E2)$ values at $N = 32$.

*Key words:* Radioactive beams, relativistic Coulomb excitation, transition probabilities, shell model
*PACS:* 27.40.+z, 25.70.De, 23.20.Ck, 21.60.Cs

Nuclei far off the valley of stability have become more accessible in recent years through the use of radioactive ion beams. The investigation of shell structures of such nuclei is a key topic of nuclear structure studies. It has become evident that shell and subshell closures may differ significantly from those of nuclei near stability, in particular for very neutron-rich nuclei [1]. However, experimental data, needed to test and refine the interactions used in the shell model calculations [2–5], are still scarce. Modifications of the shell structure have far reaching consequences for nuclear properties and also beyond nuclear structure physics, e.g. for the rapid neutron-capture process (r-process) of stellar nucleosynthesis and the resulting isotopic abundances [6].

The experimental evidence of changing shell structures for very neutron-rich nuclei along the $N = 8$, 20 and 28 isotonic sequences can be explained in terms of the monopole part of the nucleon-nucleon (NN) residual interaction. Schematically this is due to the $(\sigma\sigma)(\tau\tau)$ term in the interaction, where $\sigma$ and $\tau$ denote the spin and isospin operators, respectively. This term is strongly binding in the $S = 0$ (spin-flip), $\Delta l = 0$ (spin-orbit partners) and $T = 0$ (proton-neutron) channel of the two-body interaction. It causes large monopole shifts of neutron single-particle orbitals due to their missing $S = 0$ proton partners at large neutron excess and, thus, may generate new shell gaps. The effect was first discussed for the (s,d) shell [2,3] and for the (p,f)

* Corresponding author.
*Email address:* hubel@hiskp.uni-bonn.de (H. Hübel).

shell [1,3]. For heavier nuclei the tensor part of the NN interaction creates a likewise strong monopole interaction between $S = 0$, $\Delta l = 1$ and $T = 0$ orbits of adjacent harmonic oscillator shells [7,8], which plays a key role in the evolution of the spin-orbit splitting. It has recently been shown, that both terms originate from the tensor force which, in a major shell with fixed parity, reduces essentially to the $(\sigma\sigma)(\tau\tau)$ term [8]. To date the investigations concentrate, in the region of neutron-rich Ca, Ni and Sn isotopes, on the most significant matrix elements, the spectroscopic factors and the magnetic moments which are sensitive indicators of their structure.

The neutron-rich Cr isotopes are located at a key point on the pathway from the $N = 40$ subshell closure via a deformed region to spherical nuclei at $N = 28$. Two large-scale shell model calculations have been performed based on different realistic effective interactions with empirically tuned monopoles [9,10]. The results await experimental proof with respect to model space and evolution of subshells and deformation. Experimentally, a possible subshell closure at $N = 32, 34$ seems to develop in the Ca isotopes beyond $N = 28$ as indicated by a rise in the $2_1^+$ energies. The Cr and Ti isotopes show a maximum of those energies at $N = 32$ [4,11–14]. However, the Ni isotopes do not show such an effect. Within the $N = 34$ isotones, $E(2_1^+)$ is increasing from Fe to Cr in contrast to the expected trend towards mid-shell, which may suggest an $N = 34$ closure [4]. Besides the $2_1^+$ energies, masses and $B(E2)$ values are an important test of the evolution of the subshell structure. A recent determination of $B(E2, 0^+ \rightarrow 2_1^+)$ values in $^{52,54,56}$Ti confirms the subshell closure at $N = 32$, but provides no evidence for the predicted $N = 34$ closure [15]. The measurement of $B(E2)$ values for the $N = 32$ and 34 isotopes of Cr, which is the subject of the present investigation, confirms the $N = 32$ subshell closure for $Z = 24$.

Three consecutive experiments were performed to measure Coulomb excitation of high-energy $^{54}$Cr, $^{56}$Cr and $^{58}$Cr beams using the FRS-RISING setup at GSI [16]. The setup is shown schematically in Fig. 1. Fully stripped Cr ions were produced by fragmentation of a $^{86}$Kr beam on a $^{9}$Be production target with a thickness of $2.5\,\mathrm{g/cm^2}$ placed in front of the fragment separator FRS. The $^{86}$Kr beams with energies of around $480A$ MeV and an intensity of 3 to $10 \times 10^8$ ions per second were provided by the heavy-ion synchrotron SIS. The nuclei of interest were selected in the FRS by their magnetic rigidity, $B\rho$, and their specific energy loss in the degraders, $\Delta E$. The various detectors on the way to the reaction target, see Fig. 1, were used to perform $A$ and $Z$ identification as well as position tracking [16]. Table 1 summarises the beam times and the intensities and compositions of the beams obtained in each of the three experiments.

The energies of the Cr beams were adjusted to around $136A$ MeV before the reaction target, a $7 \times 7\,\mathrm{cm^2}$ Au foil of $1\,\mathrm{g/cm^2}$ thickness, in which the ions

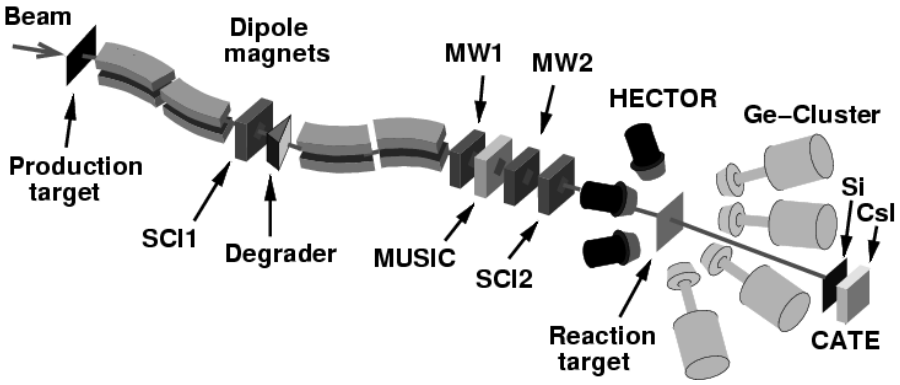


Fig. 1. Schematic illustration of the RISING setup at the fragment separator, FRS, at GSI. The $BaF_2$ scintillation spectrometers of the HECTOR array were used only in the setup phase. An additional degrader, which was placed between the first two dipole magnets, is not shown.

Table 1
Summary of beam times, beam intensities and compositions for the three experiments.

| Isotope | Beam Time [h] | Intensity [$s^{-1}$] | $^{A}$Cr Component [%] | Other Main Comp. |
|---|---|---|---|---|
| $^{54}$Cr | 22 | 2000 | 45 | $^{55}$Mn, $^{53}$V |
| $^{56}$Cr | 20 | 1400 | 35 | $^{57}$Mn, $^{55}$V |
| $^{58}$Cr | 55 | 600 | 25 | $^{59}$Mn, $^{57}$V |

were slowed down to $100A$ MeV in all three experiments. The identification of the nuclei behind the reaction target in $Z$ and $A$ is performed by the array of nine Si and CsI(Tl) detectors of the calorimeter telescope CATE [17]. The $Z$ resolution of CATE is good, but masses of neighbouring isotopes partly overlap.

Gamma rays emitted after Coulomb excitation were measured in the array of 15 Ge-Cluster detectors of the RISING setup [16]. Due to the high recoil velocities of $v/c \approx 0.43$, the Doppler broadening of the $\gamma$-ray lines is appreciable. To maintain a good energy resolution, the Ge detectors were placed at forward angles with a small opening angle of 3°. The photopeak efficiency of the Cluster array was 1.13(1) % at 1.33 MeV, measured with a $^{60}$Co source. However, the solid angle transformation increases the efficiency to 2.3 % for $\gamma$ rays emitted from the high-energy Cr ions. To reduce background contributions, the Cluster detectors were surrounded at the sides by lead shielding of 6 mm thickness. Thinner Pb absorbers were used in front of the detectors to suppress $\gamma$ rays with energies below 500 keV in the laboratory frame.

Particle-gamma coincidences were recorded requiring a $\gamma$ ray in one or more of the Ge detectors, an incoming particle in scintillator SCI2 and an outgoing

particle in one of the CsI detectors of CATE. To determine the number of beam particles, events without $\gamma$-ray coincidence condition were recorded. In the off-line analysis event-by-event tracking and identification of the incoming ions was performed. For the correction of Doppler shifts of the $\gamma$-ray energies, the trajectory of each incoming Cr projectile, the position of the scattered particle measured in CATE and the position of the Ge crystal detecting a $\gamma$ ray were used to determine the $\gamma$-ray emission angle with respect to the direction of the scattered projectile. The ion velocities after the target were calculated for each event from the time of flight between the two scintillation detectors, SCI1 and SCI2, taking the energy loss in the Au target into account. After Doppler correction, an energy resolution of 2 % was obtained. The accepted scattering angles of the Cr fragments were limited to the range of 0.6° to 2.8° to select predominantly Coulomb-excitation events. This range of scattering angles corresponds to impact parameters between 10 fm (below which nuclear reactions prevail) and 50 fm (above which atomic background becomes dominant).

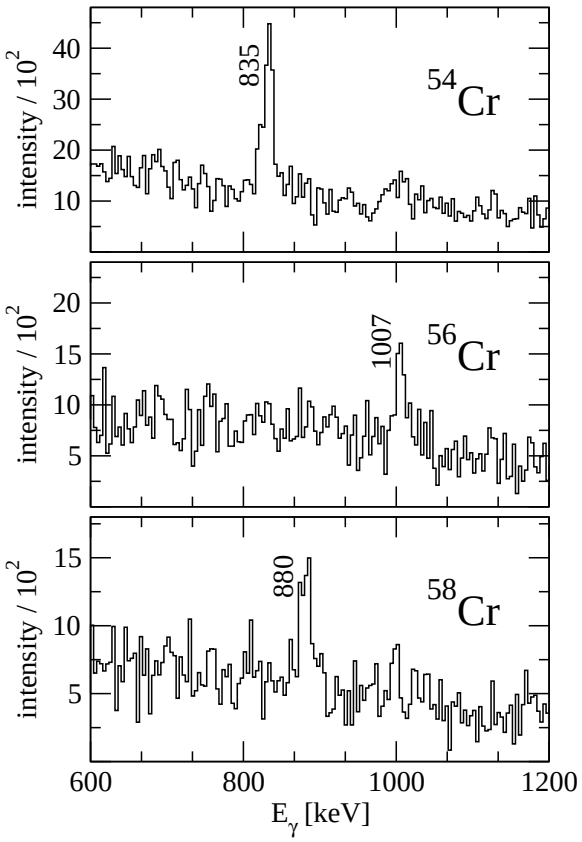


Fig. 2. Examples of Doppler- and efficiency-corrected $\gamma$-ray spectra showing the $2_1^+ \rightarrow 0^+$ transitions in $^{54,56,58}$Cr.

Examples of the $\gamma$-ray spectra obtained for the three Cr isotopes are displayed in Fig. 2. They were obtained after event-by-event correction for Doppler shifts and for the efficiencies of the individual Ge detectors. Isotope identification

Table 2
Gamma-ray energies ($E_\gamma$), number of counts in the $2_1^+$ peaks ($N_\gamma$), $\gamma$-ray intensities ($I_\gamma$), number of projectiles identified as Cr before and after the target ($N_{\rm pro}$) and $B(E2; 2_1^+ \rightarrow 0^+)$ values for $^{54,56,58}$Cr.

| Isotope | | $^{54}$Cr | $^{56}$Cr | $^{58}$Cr |
|---|---|---|---|---|
| $N_{\rm pro}$ | [$10^6$] | 37 | 18 | 12 |
| $N_\gamma$ | | 501(64) | 126(44) | 148(43) |
| $I_\gamma$ | [$10^2$] | 211(27) | 61(20) | 73(19) |
| $B(E2)$ | [W.u.] | 14.6(0.6)[a] | 8.7(3.0) | 14.8(4.2) |
| $E(2_1^+)$ | [keV] | 835[a] | 1007[a] | 880[b] |

[a] from ref. [18] [b] from ref. [4]

was made before and after the Au target and a prompt time gate was set to reduce the background from $\gamma$ rays produced at various places along the beam line. The gate widths were varied within reasonable limits. A variation in the number of counts in the resulting spectra was taken into account in the uncertainties. Other peaks in the spectra originate from neighbouring Cr isotopes produced by transfer reactions which cannot be completely separated due to the insufficient mass resolution after the target. However, these contaminations do not influence the results as they represent a negligible fraction of the number of projectiles, $N_{\rm pro}$, which is the number of projectiles within the scattering-angle range identified as Cr both before and after the target. The other ions, mainly Mn and V, present in the beam do not give rise to contaminations in the spectra since they are well separated from the gates on the Cr ions.

The $\gamma$-ray transition intensities, $I_\gamma$, were obtained by integrating over the $2_1^+ \rightarrow 0^+$ peaks in the three spectra and subtracting the background. Angular distribution effects, which should be identical for the three Cr isotopes, were not taken into account. In principle, $B(E2)$ values could be determined from the Coulomb-excitation cross sections for the three isotopes [19,20]. However, to avoid possible systematic errors, e.g. from uncertain parameters in the high-energy Coulomb excitation calculation, from possible excitations of higher-lying $2^+$ states (for which we see no evidence in the spectra) or from unknown angular distribution effects, we prefer to give the $B(E2)$ values for $^{56}$Cr and $^{58}$Cr relative to the previously known value of $^{54}$Cr, see Table 2. The $B(E2)$ values for $^{56,58}$Cr are determined using the relation:

$$B(E2, {}^{\rm A}{\rm Cr}) = \frac{I_\gamma({}^{\rm A}{\rm Cr})/N_{\rm pro}({}^{\rm A}{\rm Cr})}{I_\gamma({}^{54}{\rm Cr})/N_{\rm pro}({}^{54}{\rm Cr})} B(E2, {}^{54}{\rm Cr}).$$

In Fig. 3 the experimental $2_1^+$ excitation energies, $E(2_1^+)$, and the $B(E2, 2_1^+ \rightarrow 0^+)$ values for the Cr isotopes are displayed. The $B(E2)$ values show that the

collectivity of the $2_1^+$ state in $^{56}$Cr with $N = 32$ is significantly lower than that of the neighbouring isotopes, $^{54}$Cr and $^{58}$Cr with $N = 30$ and 34, respectively. In fact, it appears to be similar to that of $^{52}$Cr with the $N = 28$ shell closure. The experimental values are compared to results of large-scale shell model

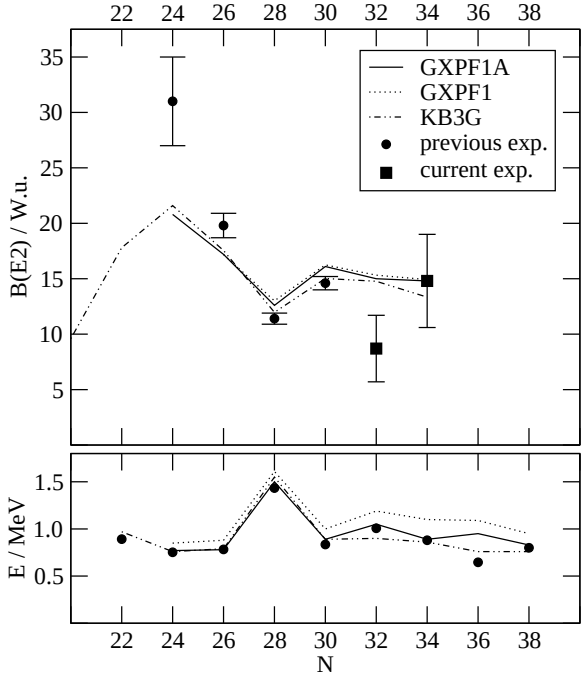


Fig. 3. Calculated (from [8–10]) and experimental energies (from [4,18]), $E(2_1^+)$, and $B(E2, 2_1^+ \rightarrow 0^+)$ values (from [18] and this work) for Cr isotopes.

calculations using two different approaches. In the calculations the effective NN interactions `GXPF1` [9] and `KB3G` [10], respectively, were used in the (p,f) model space. The $B(E2)$ values were calculated with equal polarisation charges for protons and neutrons, $\delta e = 0.5e$. For $N \geq 36$ the $\nu(\mathrm{g}_{9/2}, \mathrm{d}_{5/2})$ orbitals were included in ref. [10] to account for the onset of deformation expected due to the upward monopole drift of the $\nu\mathrm{f}_{5/2}$ orbital which closes the $N = 40$ gap. However, up to $N = 36$ little effect is predicted as compared to the (p,f) model-space values. The `GXPF1` interaction was recently modified (`GXPF1A`) to better account for the $E(2_1^+)$ energies in Ti and Cr isotopes, but with marginal effect for the $B(E2)$ values (see Fig. 3) [8]. The interactions `GXPF1` and `KB3G` differ mainly in the prediction of an $N = 34$ subshell in $^{54}$Ca, which is only produced by `GXPF1`. The difference can be traced back to the $\nu(\mathrm{p}_{1/2})^2$ $T = 1$, $J = 0$ two-body matrix element which is not related to the tensor interaction. It is strongly binding in `GXPF1A` [8] and stabilises the $N = 32$ and 34 shell gaps with the $\nu\mathrm{p}_{1/2}$ subshell filled in between. The situation is analogous to the (s,d) shell for $N = 14, 16$ in $^{22,24}$O and $Z = 14, 16$ in $^{34}$Si, $^{36}$S and to the proton (p,f) shell in the $N = 50$ isotones $^{88}$Sr, $^{90}$Zr at $Z = 38, 40$ [7]. Despite the variations in the $E(2_1^+)$ energies, the $B(E2)$ values are virtually unchanged in both shell model approaches and are almost constant from $N = 30$ to 34 (see Fig. 3). The experimental value for $^{56}$Cr clearly lies below the theoretical predictions.

The small $B(E2)$ value is evidence for the $N = 32$ subshell closure already indicated by the higher $2_1^+$ energy. This result is in agreement with a recent measurement of $B(E2)$ values in $^{52,54,56}$Ti [15] which also show a decrease in collectivity for $^{54}$Ti with $N = 32$. Further inspection of the shell model results reveals that the effective gap between the $p_{3/2}$ and $p_{1/2}$ neutrons stays constant at a value of about 2 MeV for both interactions when going from Ca to Cr, in agreement with the experimental $B(E2)$ trend. The $f_{5/2}$ - $p_{1/2}$ gap decreases from 3.5 MeV in Ca to 1.5 MeV in Cr for `GXPF1A` while it disappears for `KB3G` [8]. This explains the fact that the $N = 34$ gap has not developed in Cr and Ti, which makes Ca the crucial experimental benchmark. It also accounts for the agreement within the two theoretical approaches for Cr and Ti. The experimental trend of the $B(E2)$ values implies that the $p_{3/2}$ - $p_{1/2}$ gap is larger than predicted while the $f_{5/2}$ - $p_{1/2}$ gap is smaller than inferred from the `GXPF1` interactions. The $B(E2)$ values in the $N = 32, 34$ Cr isotopes must also be seen in the light of a comparison to the shell model values for the Fe and Ni isotopes [10] which show the normal peaking in the ($p$,$f_{5/2}$) mid-shell at $N = 32 - 34$. A further test of the model predictions would be a study of the heavier Cr isotopes which should show a steep increase in the $B(E2)$ values towards deformation.

The authors wish to thank the technical staff at GSI for providing the Cr beams. The work was supported by the German BMBF under grant nos. 06BN-109, 06OK-167 and by the Polish State Committee for Scientific Research (KBN grant no. 620/E-77/SPB/GSI/P-03/DWM105/2004-2007).

## References

[1] H. Grawe, Acta Phys. Pol. B **34**, 2267 (2003).

[2] T. Otsuka *et al.*, Phys. Rev. Lett. **87**, 082502 (2001).

[3] T. Otsuka *et al.*, Eur. Phys. J. A **13**, 69 (2002).

[4] J. I. Prisciandaro *et al.*, Phys. Lett. B **510**, 17 (2001).

[5] A. P. Zuker, Phys. Rev. Lett. **90**, 042502 (2003).

[6] B. Pfeiffer *et al.*, Nucl. Phys. A **693**, 282 (2001).

[7] H. Grawe, Springer Lect. Notes Phys. **651**, 33 (2004).

[8] T. Otsuka *et al.*, Acta Phys. Pol. B **36**, 1213 (2005).

[9] M. Honma *et al.*, Phys. Rev. C **69**, 034335 (2004).

[10] E. Caurier *et al.*, Eur. Phys. J. A **15**, 145 (2002).

[11] R. V. F. Janssens *et al.*, Phys. Lett. B **546**, 55 (2002).

[12] B. Fornal *et al.*, Phys. Rev. C **70**, 064304 (2004).

[13] S. Liddick *et al.*, Phys. Rev. C **70**, 064303 (2004).

[14] S. N. Liddick *et al.*, Phys. Rev. Lett. **92**, 072502 (2004).

[15] D.-C. Dinca *et al.*, Phys. Rev. C **71**, 041302 (2005).

[16] H. Wollersheim *et al.*, Nucl. Instr. Meth. A **537**, 637 (2004).

[17] R. Lozeva *et al.*, Acta Phys. Pol. B **36**, 1245 (2005).

[18] ENSDF database, `http://www.nndc.bnl.gov/ensdf/`.

[19] T. Glasmacher, Nucl. Phys. A **693**, 90 (2001).

[20] C. Bertulani *et al.*, Comp. Phys. Comm. **152**, 317 (2003).